Modulation of the *Shaker* K^+ Channel Gating Kinetics by the S3–S4 Linker

Carlos Gonzalez,*‡ Eduardo Rosenman,*‡ Francisco Bezanilla,§¶ Osvaldo Alvarez,*‡ and Ramon Latorre*‡¶

From the *Centro de Estudios Cientificos de Santiago, Presidente Errazuriz 3132, Santiago, 6760470 Chile; ‡Departmento de Biologia, Facultad de Ciencias, Universidad de Chile, Santiago, 6850240 Chile; and the §Department of Physiology and ¶Department of Anesthesiology, University of California, Los Angeles, School of Medicine, Los Angeles, California 90095

abstract In *Shaker* K^+ channels depolarization displaces outwardly the positively charged residues of the S4 segment. The amount of this displacement is unknown, but large movements of the S4 segment should be constrained by the length and flexibility of the S3–S4 linker. To investigate the role of the S3–S4 linker in the *Shaker*H4Δ(6–46) (*Shaker*Δ) K^+ channel activation, we constructed S3–S4 linker deletion mutants. Using macropatches of *Xenopus* oocytes, we tested three constructs: a deletion mutant with no linker (0 aa linker), a mutant containing a linker 5 amino acids in length, and a 10 amino acid linker mutant. Each of the three mutants tested yielded robust K^+ currents. The half-activation voltage was shifted to the right along the voltage axis, and the shift was +45 mV in the case of the 0 aa linker channel. In the 0 aa linker, mutant deactivation kinetics were sixfold slower than in *Shaker*Δ. The apparent number of gating charges was 12.6 ± 0.6 e_o in *Shaker*Δ, 12.7 ± 0.5 in 10 aa linker, and 12.3 ± 0.9 in 5 aa linker channels, but it was only 5.6 ± 0.3 e_o in the 0 aa linker mutant channel. The maximum probability of opening (P_o^{max}) as measured using noise analysis was not altered by the linker deletions. Activation kinetics were most affected by linker deletions; at 0 mV, the 5 and 0 aa linker channels' activation time constants were 89× and 45× slower than that of the *Shaker*Δ K^+ channel, respectively. The initial lag of ionic currents when the prepulse was varied from −130 to −60 mV was 0.5, 14, and 2 ms for the 10, 5, and 0 aa linker mutant channels, respectively. These results suggest that: (a) the S4 segment moves only a short distance during activation since an S3–S4 linker consisting of only 5 amino acid residues allows for the total charge displacement to occur, and (b) the length of the S3–S4 linker plays an important role in setting *Shaker*Δ channel activation and deactivation kinetics.

key words: *Shaker* K^+ channel • S3-S4 linker • S4 displacement

INTRODUCTION

The opening of *Shaker* K^+ channels is associated with the displacement of ~13 electron charge units (Schoppa et al., 1992) or ~3.3 e_o per subunit since the channel is a tetramer (MacKinnon, 1991; Liman et al., 1992). In voltage-dependent K^+ channels, several studies indicate that most of these charges are confined to the fourth transmembrane domain (S4) of the channel protein (Aggarwal and MacKinnon, 1996; Seoh et al., 1996). The S4 segment contains several highly conserved positively charged amino acids. In *Shaker* K^+ channels, at least four of these residues contribute to the voltage sensitivity of the channel and to the gating currents: arginines 362, 365, 368, and 371. Transmembrane displacements of the S4 domain were detected in K^+ and Na^+ channels using cysteines substituting residues in S4 (Larsson et al., 1996; Yusaf et al., 1996; Yang and Horn, 1995; Yang et al., 1996). These studies showed that the accessibility of these amino acid residues changes as the channel undergoes transitions between closed, open, and inactivated states. Moreover, when attached to specific sites near the S4 segment of the *Shaker* K^+ channel, the fluorescence probe tetramethylrhodamine maleimide undergoes voltage-dependent changes in intensity that correlate with the movement of the voltage sensor (Mannuzzu et al., 1996; Cha and Bezanilla, 1997). More recently, Starace et al. (1997) and Starace and Bezanilla (1998, 1999) showed that when arginines 362, 365, 368, and 371 are replaced by histidines, they move from the internal to the external aqueous environment of the channel during activation resulting in passive proton transport across the membrane. These experiments support the idea of the presence of narrow vestibules that line the S4 segment, allowing the passage of protons but excluding the larger cysteine reactive reagents (compare Larsson et al., 1996).

All the evidence given above points to the fact that the S4 transmembrane domain is an important part of the voltage sensor and that this domain of the protein moves in the electric field when the channel is activated by voltage. According to some models, the S4 segment moves during channel activation across the membrane as a sliding helix (Durell and Guy, 1992; Catter-

Address correspondence to Dr. F. Bezanilla, Dept. of Physiology, UCLA School of Medicine, 10833 Le Conte Avenue, Los Angeles, CA 90095. Fax: 310-794-9612; E-mail: fbezanil@ucla.edu

all, 1996). In this model, the helical screw movement is perpendicular to the lipid bilayer. Therefore, the displacement of the S4 segment that involves transfer of at least 10 amino acid residues (362–371) across the membrane is on the order of 1.5 nm. With such a large movement, the S4 segment displacement should be constrained by the length of the S3–S4 linker. On the other hand, several investigators have proposed that the electric field can be focused in a region of the membrane much narrower than the bilayer thickness. If this is the case, only small conformational changes of the voltage sensor would be necessary to translocate the gating charges through the entire electric field (Larsson et al., 1996; Seoh et al., 1996; Yang et al., 1996; Papazian and Bezanilla, 1997). In this case, the length of the S3–S4 linker would not be critical for the sensor operation. One study that can shed some light about the actual extent of the displacement of the S4 segment is to measure the gating properties of *Shaker* K^+ channel mutants with an S3–S4 linker of different lengths.

The role of the S3–S4 linker in *Shaker* K^+ channel activation was previously studied by Mathur et al. (1997). They defined the S3–S4 linker as the 25 amino acid segment comprised between glutamate 333 and serine 357 and found that changes in charge and length of the S3–S4 linker produced only minor effects in the voltage dependence of activation. In the present study, we have used the alignment of voltage-dependent K^+ channels done by Wallner et al. (1996) and redefined the S3–S4 linker to be the segment comprised of amino acid residues valine 330 to isoleucine 360 (Fig. 1). According to this new definition, the S3–S4 linker is a 31 amino acid (aa)[1] segment. To study the role of this segment in *Shaker* K^+ channel activation, we have characterized in detail three deletion mutants: one in which the linker was completely deleted (0 aa), a second one in which 5 amino acid residues from the carboxy terminus were left (5 aa linker), and a mutant in which the S3–S4 linker contains 10 noncontiguous amino acid residues (10 aa linker) (Fig. 1).

We found that after complete deletion of the S3–S4 linker, fully functional channels are expressed, although the details of channel voltage-dependent activation are different from that of the wild type. We conclude that the S4 segment needs to move only a short distance to signal the ion pathway to open.

MATERIALS AND METHODS

Mutations and Channel Expression

Constructs were prepared on *Shaker*H4Δ(6-46) (*Shaker*H4Δ). The deletion of amino acid residues from 6 to 46 removes N-type inactivation. The *Shaker*H4Δ K^+ channel cDNA was originally cloned into an engineered version of the pBSTA vector. The S3–S4 deletion mutants were *Shaker*H4Δ-Δ(330-360), dubbed here 0 aa linker, *Shaker*H4Δ-Δ(330-355) (5 aa linker), and *Shaker*H4Δ-Δ(332-351) (10 aa linker), and were prepared by PCR-based mutagenesis (Expand Hi Fidelity PCR system; Boehringer Mannheim, or Pfu DNA polymerase; Stratagene). The S3–S4 linker was defined as the segment comprised of residues 330–360 (Fig. 1; Wallner et al., 1996). Primers (Oligopéptido; Santiago7) were designed to give a product containing the complete cDNA sequence except for the deleted sequence described above. The PCR products were purified by agarose gel electrophoresis, phosphorylated using T4 polynucleotide kinase (GIBCO BRL, Life Technologies, Inc.) and ligated using T4 DNA ligase (GIBCO BRL, Life Technologies, Inc.).

Competent *Escherichia Coli* cells, DH5 or XLI Blue, were transformed with the ligation products. Colonies obtained after transformation were selected using HaeII (one cut at the S3–S4 linker). cDNAs from preselected colonies were sequenced using T7 Sequenase version 2.0 (Amersham) to choose those having the expected sequence. The ~400-bp cassettes containing the mutations were cut out using the restriction enzymes XbaI and BsmI and were subcloned in the vector pBSTA with the original *Shaker*H4Δ DNA insert. The mutated cDNAs were transcribed in vitro using T7 RNA polymerase (mMessage Machine; Ambion). Transcription was done at 37°C in a volume of 10 μl, following the manufacturer's instructions. The cRNA products were extracted with ethanol, and suspended in double distilled water to a final concentration of 1 μg/μl.

Translation of the cRNA's was done in *Xenopus laevis* oocytes. Xenopus were purchased from Nasco International, Inc. The protocol used to isolate *Xenopus laevis* oocytes received institutional approval and followed National Institutes of Health guidelines. Oocytes from *Xenopus laevis* were defolliculated by incubation with 2.5 mg/ml collagenase in filtered OR-2 medium. Oocytes were well separated after shaking 1–2 h on a clinical rotator at room temperature at 180 rpm (ROT-2; P+L Electrónica). Collagenase was removed by washing the separated oocytes five times with OR-2 medium containing (mM): 82.5 NaCl, 2.5 KCl, 1 $MgCl_2$, 5 HEPES, pH 7.6, and five times with ND-96 medium containing (mM): 96 NaCl, 2 KCl, 1 $MgCl_2$, 1.8 $CaCl_2$, 500 mg/ml gentamicin, 5 HEPES, pH 7.6. Collagenase was from GIBCO BRL Life Technologies, Inc. Stage V and VI oocytes were selected and maintained in ND-96 medium at 18°C for 12–24 h before RNA injection. 50 nl of cRNA solution (0.1–0.2 μg/μl) was injected into either the vegetal or the animal poles of each oocyte using micropipettes (4878; World Precision Instruments) of 20-μm tip diameter attached to a microinjector (A203XVY; World Precision Instruments).

Electrophysiology

2–5 d after cRNA injection and after the manual removal of the vitelline membrane, currents elicited by the different mutants were recorded in cell-attached macropatches of oocyte membrane. Patch pipettes of 10–30 μM in diameter were pulled from melting point tubes (9530-1; Corning Glass Works) and had a resistance of ~1 MΩ. No series resistance compensation was used and the error due to uncompensated series resistance was never greater than 5 mV. Bath and pipette solutions contained (mM): 110 KMES, 10 HEPES, 2 $CaCl_2$, pH 7.2. The acquisition and basic analysis of the data were performed with pClamp 6.0 software (Axon Instruments, Inc.) driving a 12-bit analogue interface card (Labmaster DMA; Scientific Solutions, Inc.).

Macroscopic Current Analysis

For macroscopic current relaxation experiments, the membrane was held at −100 mV. Each experimental episode consisted of an epoch at the holding potential, followed by a depolarization to

[1]*Abbreviations used in this paper:* aa, amino acid; WT, wild type.

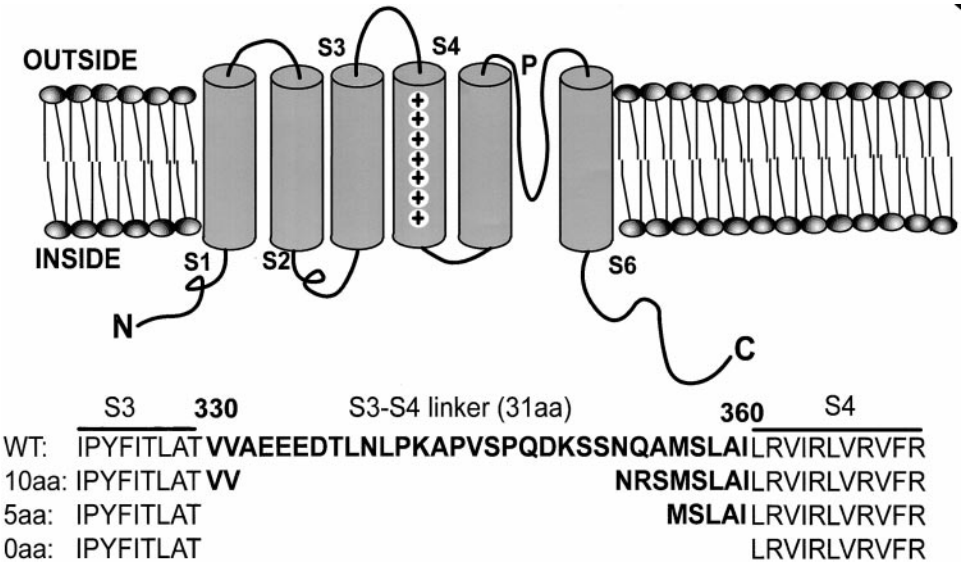

Figure 1. Mutations of the *Shaker* S3–S4 linker region. The wild-type *Shaker* sequence (top) is compared with the mutations studied here. The S3–S4 linker was defined according to Wallner et al. (1996). The asparagine-arginine-serine sequence in the 10 aa linker channel corresponds to the S3–S4 linker region present in the human calcium-activated K^+ channel (h*Slo*; Wallner et al., 1996).

different test voltages and ending with an epoch at −60 mV. The episode duration ranged from 140 to 1,400 ms, depending on the relaxation times of the various mutant channels. Each experiment consisted of 10–50 episodes separated by 1–2 s. The test pulse was incremented by 3–10 mV on each subsequent episode. For each episode, 512 digital samples of current were acquired at equally spaced times. The analogue signal was filtered before digitization with an eight-pole low-pass Bessel filter with a cutoff frequency of 1/5 of the conversion frequency. Conductance–voltage relations were determined from the peak amplitude of the tail currents after repolarization to a fixed negative voltage.

Cole-Moore Analysis

Families of currents from the WT *Shaker*Δ and linker mutant channels were obtained as follows: 100-ms-long prepulses to voltages between −130 and −40 mV preceded pulses to +50 mV. Each current record obtained during the 50-mV pulse was compared with the current record measured after the −130-mV prepulse. Records were displaced along the time axis and the differences were evaluated visually. The time displacement giving the best superposition of the traces was taken as the Cole-Moore shift.

Time Constants Calculation

A quantitative comparison of the activation kinetics was obtained from monoexponential fits of the upper 50% of the rising phase of the current. The mathematical expression used for the fit of the time course of channel activation was:

$$I(t) = 0 \text{ (for } \tau < d)$$
$$I(t) = I_{max}\{1 - \exp[-(t-d)/\tau_a]\} \text{(for } t > d), \quad (1)$$

where d is the delay and t the time constant of the exponential. This simplified approach has been demonstrated to be efficient for assessing rate constants in multistep ramified activation pathways (Schoppa and Sigworth 1998a). For large depolarizations, where the backward rate constants are negligible, the parameter τ_a is a measure of the reciprocal value of the slowest rate constant in the activation path and d is a measure of the addition of the reciprocal values of all the rest of the constants.

Deactivation kinetics were obtained by fitting the early decay of the tail current to a sum of two monoexponential decays, leaving out the first 0.1 ms of the test pulse to allow for clamp settling. The fastest time constant of the decay of the tail currents was used as an estimation of the rate constant of closing (deactivation) of channels.

Variance Analysis

A series of identical records were recorded pulsing to a positive voltage from the holding potential. Pairs of M subsequent records $X_i(t)$, $X_{i+1}(t)$ were subtracted to compute the experimental nonstationary ensemble variance. The average basal variance at the holding voltage was subtracted from the variance obtained during the test pulse. The subtracted variance (σ^2) was plotted versus mean current [I(t)] and the data was fitted using (Sigworth, 1980):

$$\sigma^2 = iI(t) - I(t)^2/N, \quad (2)$$

where i is the single channel current amplitude and N the number of channels. i was obtained from the initial slope, N was obtained from the nonlinear curve fitting analysis done under Microsoft Excel. The maximum open probability, P_o^{max} was obtained according to the relation: $P_o^{max} = I_{max}/iN$ where I_{max} is the maximum mean current measured in the experiment.

Limiting Slope Analysis

The method developed by Almers (1978) gives the number of effective gating charges coupled to the channel opening in a sequential model with any number of closed states and only one open state. However, the method is also valid for any nonsequential or sequential model having one or more than one open state as long as the transitions between open states are voltage independent (Sigg and Bezanilla, 1997). The ionic current recorded during a voltage ramp was subtracted off line from the linear leakage and subsequently converted into conductance by dividing the ionic current by its driving force. The G-V plot was fitted to a monoexponential approximation in the limit of very negative voltages:

$$G(V) = A\exp(z\delta FV/RT), \quad (3)$$

where z is the number of effective charges per channel. The $z\delta$ value was also obtained from the relationship:

$$z\delta(V) = (kT/e_o)d\ln G(V)/dV. \quad (4)$$

As pointed out by Zagotta et al. (1994a), a plot of $z\delta$ as a function of voltage (or P_o) is a good test of having reached the true limiting slope. In this plot, at very negative voltages, $z\delta$ will asymptotically approach a saturating value that is equal to the total number of charges per channel.

In the text, errors in all measured quantities are given as mean ± SD.

RESULTS

Deletions at the Amino-Terminal End of the S3–S4 Linker Slow Down the Rates of Channel Activation and Deactivation

Fig. 2 shows ionic currents elicited by various depolarizing voltages from a holding voltage of −100 mV followed by a postpulse to −60 mV for the *Shaker*Δ "wild type" (WT) (Fig. 2 A) channel. Ionic currents records for the 10, 5, and 0 aa S3–S4 linker channel mutants are shown in Fig. 2, B, C, and D, respectively. Robust K^+ currents from each deletion mutant 1 or 2 d after the cRNA injection implied that none of the mutations in the S3–S4 linker affected the synthesis and assembly of the functional *Shaker*Δ K^+ channels in oocyte membranes. Complete (0 aa linker) or partial (5 aa linker) removal of the linker profoundly affected the rates of channel activation. The 10 aa linker mutant has biophysical properties very similar to those of the WT channels. Both activation and deactivation kinetics were slowed down in the 0 aa linker channel compared with the wild-type channel (Fig. 2 D). In Fig. 2 D, we can clearly see that in the 0 aa linker mutant the tail currents become very slow. The same phenomenon was observed in the case of the 5 aa linker mutant. However, in this case, the effect of the deletion is mainly on the activation kinetics. The time course of the ionic current in this case is very slow and at intermediate depolarizations the current increases only after a long time delay. This initial lag of ionic currents is also present in the 0 aa, but is particularly pronounced in the 5 aa linker mutant (Fig. 1 C; see also Fig. 4).

Deletions in the S3–S4 Linker Shift the Voltage–Activation Curve

Information about the mutant and WT channels' behavior under equilibrium conditions was obtained from conductance versus voltage curves. Conductance versus voltage curves for the WT and mutant channels were obtained by directly plotting the peak tail current amplitude at a constant postpulse potential (−60 mV) and as a function of the test prepulse potential in high external K^+. Notice that, at large depolarizations, the tail current saturates (e.g., Fig. 2 D), indicating that the maximum channel open probability (P_o^{max}) has been reached since the current at the peak of the tail [$I_{tail}(V)$] determined with a test prepulse V is (Eq. 5):

$$I_{tail}(V) = NiP_o(V), \quad (5)$$

where i is the current amplitude of the single channel, N the number of channels, and $P_o(V)$ the voltage-dependent open probability. Therefore, $I_{tail}(V)/I_{tail}^{max}(V) = P_o(V)/P_o^{max}$, where I_{tail}^{max} is the maximum amplitude reached by the tail currents (Stefani et al., 1994; Zagotta et al., 1994b).

Fig. 3 shows the relationships $P_o(V)/P_o^{max}$–prepulse voltage for the WT and mutant channels. Zagotta et al. (1994b) fit the conductance–voltage curves with a function of the type:

$$P_o(V)/P_o^{max} = \{1/[1 + K\exp(-z\delta FV)/RT]\}^n, \quad (6)$$

with n equal to 1 or 4, where $K\exp(-z\delta FV)/RT$ represents the voltage-dependent equilibrium constant for each independent transition. In this case, the voltage-dependent activation mechanism involves n independent conformational changes before opening. The fit to the $P_o(V)/P_o^{max}$–voltage curves using Eq. 6 is poor for the WT channel (Fig. 3 A, broken line) and is clearly inadequate for the 10 aa linker channel (Fig. 3 B, broken line). In particular, the fit to the $P_o(V)/P_o^{max}$ data, Eq. 6 misses all data points at relative open probabilities >0.8. However, the fit to the $P_o(V)/P_o^{max}$ data using Eq. 6 is good for the 5 and 0 aa linker mutants (Fig. 3, C and D; Table I). Eq. 6 is based in a model that requires only a single conformational change in each subunit to open the channel (Hodgkin and Huxley, 1952).

$$C0 \overset{1/4K}{\leftrightarrow} C1 \overset{2/3K}{\leftrightarrow} C2 \overset{3/2K}{\leftrightarrow} C3 \overset{4K}{\leftrightarrow} O \quad \text{(SCHEME I)}$$

Where C0 to C3 represent closed conformations after zero to three independent transitions, respectively, O represents the open conformation, $K = K(0)\exp(-z\delta_1 FV/RT)$ is the voltage-dependent equilibrium constant, and K(0) is the equilibrium constant at zero voltage for each transition. Scheme I corresponds to class A of models in Zagotta et al. (1994b) or 1 + 0 (each subunit undergoing one transition) in Schoppa and Sigworth (1998b) that can be summarized as $(R \leftrightarrow A)_4$— O, where each subunit can be either in a resting (R) or an active (A) conformation; we defined K = R/A.

We found that the fit to the $P_o(V)/P_o^{max}$ data improves notably for the wild type and the 10 aa linker mutant (Fig. 3, A and B, solid lines) using a model in which the four independent and identical voltage-dependent transitions are followed by a final concerted

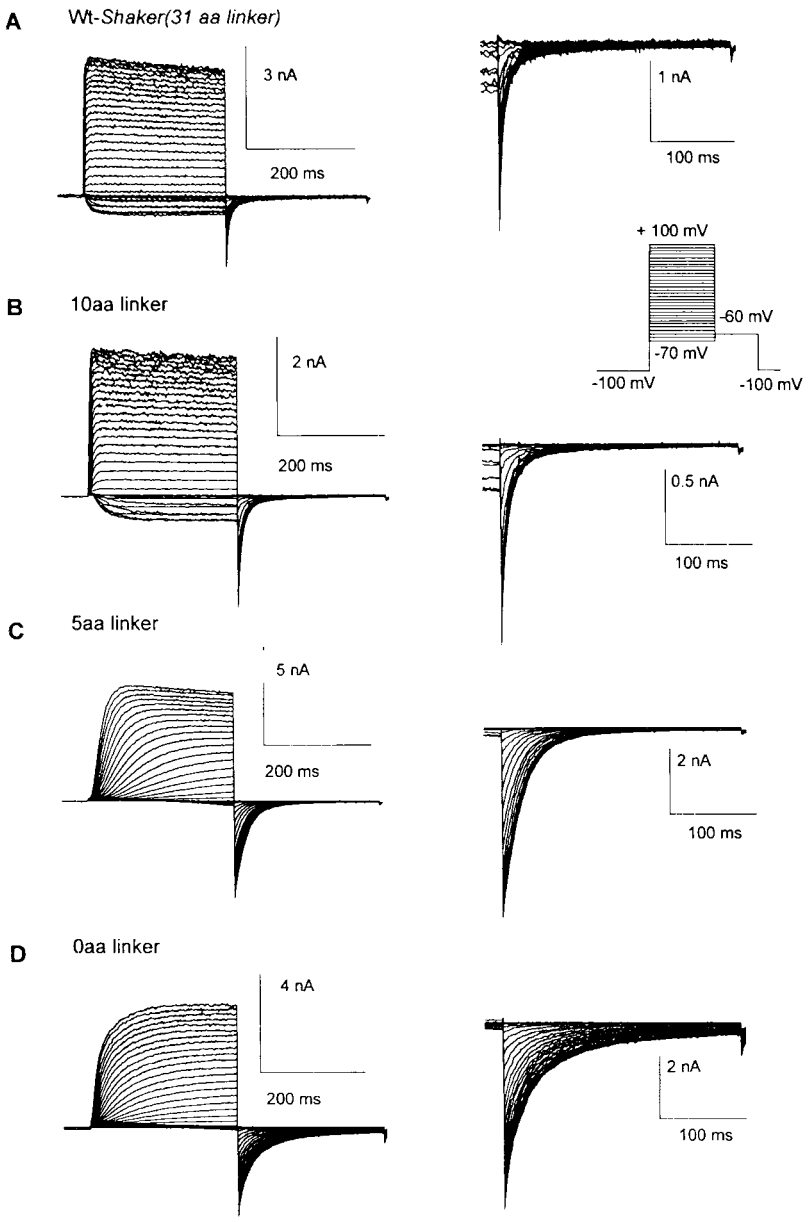

Figure 2. Deletions in the S3–S4 linker slow down activation and deactivation kinetics in *Shaker*Δ. Macroscopic currents for *Shaker*Δ (A), and 10 (B), 5 (C), and 0 (D) aa S3–S4 linker mutants. Currents were recorded from cell-attached macropatches from oocytes expressing the different channels. Currents were elicited by voltage steps from −60 to 120 mV in 5-mV increments, followed by a step to −60 mV. The holding voltage was −100 mV.

transition that lead to the open state (Koren et al., 1990; Zagotta and Aldrich, 1990) (Scheme II).

$$\underset{\text{C0}}{\overset{1/4\text{K}}{\leftrightarrow}}\ \underset{\text{C1}}{\overset{2/3\text{K}}{\leftrightarrow}}\ \underset{\text{C2}}{\overset{3/2\text{K}}{\leftrightarrow}}\ \underset{\text{C3}}{\overset{4\text{K}}{\leftrightarrow}}\ \underset{\text{C4}}{\overset{\text{Ko}}{\leftrightarrow}}\ \text{O}$$

(SCHEME II)

Where Ko represents the equilibrium constant for the concerted transition. Scheme II can be summarized as $(\text{R} \leftrightarrow \text{A})_4 \leftrightarrow \text{O}$. It is important to note here that, to fit the data for $P_o(V)/P_o^{max}$ 0.8, the concerted transition must be voltage-dependent; i.e., $\text{Ko} = \text{Ko}(0)\exp(-z\delta_2 FV/RT)$ (Table I). Recently, Ledwell and Aldrich (1999) were able to isolate the final cooperative step by taking advantage of the *Shaker* channel mutant V369I, I372L, S376T. Their results showed that the last step is voltage dependent and that the charge movement associated with the final gating transition accounts for 13% of the total charge displaced in the activation pathway.

For Scheme II, the probability of opening is given by the relation:

$$P_o(V)/P_o^{max} = (1 + \text{Ko} + 4\text{KoK} + 6\text{KoK}^2 + 4\text{KoK}^3 + \text{KoK}^4)^{-1}. \quad (7)$$

The total gating charge per channel determines the slope at very low open probabilities (e.g., Almers, 1978; Sigg and Bezanilla, 1997; see below). However, the shape and slope of the $P_o(V)/P_o^{max}$–V curves at higher open probabilities are additionally influenced by inter-

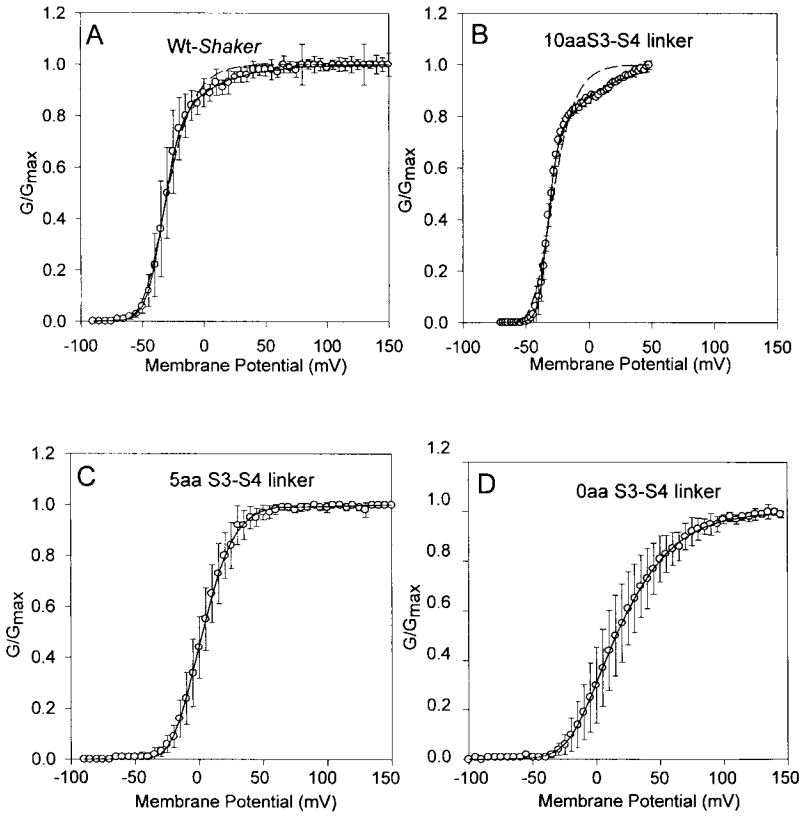

Figure 3. Deletions in the S3–S4 linker shift the G-V curves toward depolarizing voltages. Voltage dependence of activation of wild-type *Shaker*Δ and S3–S4 linker mutants. The conductance–voltage curves were obtained using tail current measurements. Each point is the average of determinations on 10–20 separate patches. Solid lines were drawn using parameters in Table I and Eq. 7 for the WT and 10 aa linker mutant, or Eq. 6 for the 5 and 0 aa linker mutants. Dashed lines drawn for the WT and 10 aa linker mutant are the best fit to a fourth power Boltzmann function.

actions between subunits (Zagotta et al., 1994a; Smith-Maxwell et al., 1998).

In the case of the 10 aa linker mutant, since the charge residues in the S4 segment were not modified, the increase in the slope (Table I) can be due to an increase in positive cooperativity between subunits. The change in slope cannot be due to an increase in the number of gating charges per channel since the limiting slope in this mutant is not different from that of the WT *Shaker*Δ channel (see below).

Why can the 5 and 0 aa linker mutants be described using a fourth power of a Boltzmann function? One possible explanation is to consider that the equilibrium $R \leftrightarrow A$ is displaced to the left in an amount such that the last concerted transition is heavily biased to the open state at those voltages that are able to displace the $R \leftrightarrow A$ to the right (all subunits in their active configuration). In other words, if we assume that linker mutations do not affect the last transition, stabilization of the subunits in the R configuration brings as a consequence that the $P_o(V)/P_o^{max}$ curves apparently behave according to Scheme I.

TABLE I

Parameters Used to Fit the Relative Open Probabilities–Voltage Curves

Parameters	WT	10 aa S3–S4 linker	5 aa S3–S4 linker	0 aa S3–S4 linker
K(0)	0.05	0.004	0.22	0.35
$z\delta_1$	1.76	2.7	1.65	0.93
Ko(0)	0.10	0.12	—	—
$z\delta_2$	0.72	0.60	—	—
n	20	20	10	10

Curves for the WT and the 10 aa linker channel were fit to Eq. 7 by least squares within the Microsoft Excel data analysis program, leaving K, $z\delta_1$, Ko, and $z\delta_2$ as adjustable parameters. $K = K(0)\exp(-z\delta_1 F/RT)$ and $Ko = Ko(0)\exp(-z\delta_2 F/RT)$. For the 5 and 0 aa linker channels, data were fit to Eq. (6). *n* is the number of experiments.

Voltage Dependence of the Activation and Deactivation Kinetics

The voltage dependence of the activation kinetics in the wild type and mutant channels was characterized by fitting the upper half of the current record to a single exponential (Fig. 4, inset) and a delay.

We fit the ionic currents obtained at depolarized voltages, where it is safe to assume that $\beta_i = 0$, using Eq. 1. The activation time constant, $\tau_a = \alpha_j^{-1}$ where α_j^{-1} is the limiting rate in Scheme III and the delay, $d = \Sigma\ \alpha_i^{-1}$ ($i \neq j$ to n). This approach is likely to be valid for branched models (Schoppa and Sigworth, 1998a).

$$C_0 \underset{\beta_1}{\overset{\alpha_1}{\leftrightarrow}} C_1 \underset{\beta_2}{\overset{\alpha_2}{\leftrightarrow}} C_2 \cdots\cdots C_{N-2} \underset{\beta_{N-1}}{\overset{\alpha_{N-1}}{\leftrightarrow}} C_{N-1} \underset{\beta_N}{\overset{\alpha_N}{\leftrightarrow}} O_N$$

(SCHEME III)

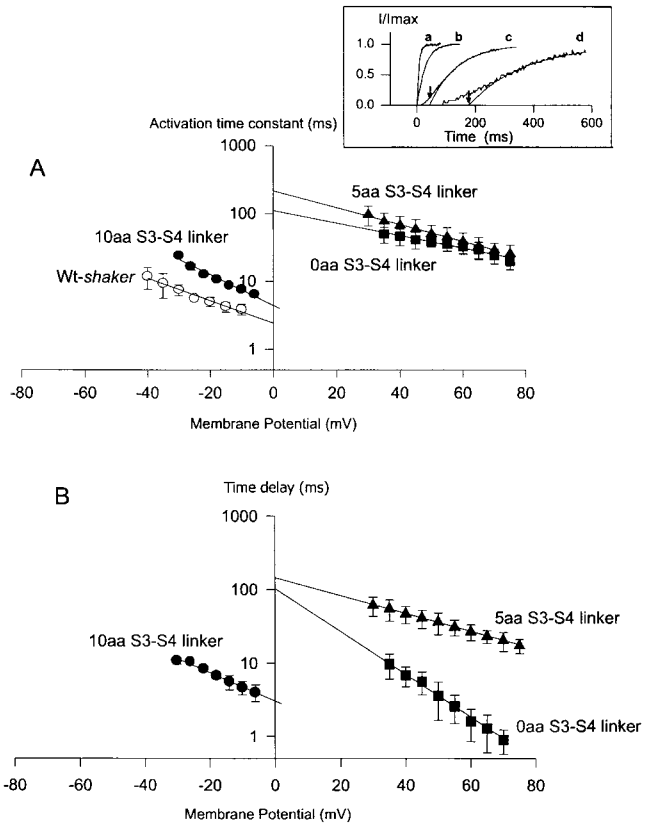

Figure 4. Activation kinetics become slower by deletions in the S3–S4 linker. (A) Channel activation was characterized by a fit of the time course of the current elicited by depolarization from a holding potential of −100 mV to and exponential function with a time constant τ_a and a time delay *d* (Eq. 1). Arrows in the inset show *d* for the 5 and 0 aa linker mutants. The fit started near the time at which current had reached ~30–50% of the maximum (see inset). Arrows in the inset show *d* for the 5 and 0 aa linker mutants. The solid lines are fits to the data using an equation of the form: $\tau_a = A \exp(-ZV/RT)$, where τ_a is the activation time constant, *A* is a constant, *Z* defines the voltage dependence of τ_a, and V is the voltage. Parameters A were 2.45 ± 0.74, 4.45 ± 0.25, 217 ± 65, and 111 ± 22 ms for the WT, and 10, 5, and 0 aa linker mutants, respectively. Parameters Z were 0.95 ± 0.35, 1.30 ± 0.03, 0.71 ± 0.08, and 0.53 ± 0.04 for the WT, and 10, 5, and 0 aa linker mutants, respectively. (B) Plots of the time delay *d* as a function of voltage. Lines were drawn using an equation of the form: $d = A \exp(-ZV/RT)$. Parameters A were 3.1 ± 1.1, 146 ± 53, and 103 ± 48 ms for the 10, 5, and 0 aa linker mutants, respectively. Parameters Z were 1.11 ± 0.10, 0.70 ± 0.05, and 1.68 ± 0.06 for the 10, 5, and 0 aa linker mutants, respectively.

In the case of the 10 aa linker mutant, τ_a at 0 mV was twofold slower than that of the WT channel. It also produced a 10-mV shift of the τ_a versus voltage curve to the right along the voltage axis (Fig. 4 A, ●). The 0 aa linker mutant resulted in a 45-fold slowing of τ_a at 0 mV compared with the WT channel and a positive shift of the τ_a versus voltage (Fig. 4 A, ■). On the other hand, the 5 aa linker mutant produced an 89-fold slowing down of activation at 0 mV (Fig. 4 A, ▲). From the slopes of the solid lines in Fig. 4 A, we calculated the number of apparent gating charges, z_a, displaced in the rate limiting transition. z_a was 1.01, 1.27, 0.71, and 0.45 for the WT, and the 10, 5, and 0 aa linker channels, respectively. Thus, shortening the S3–S4 linker from 31 to 10 aa does not modify the voltage dependence of τ_a and the complete removal of the linker induces a decrease of 0.56 in z_a. This decrease in z_a promotes a crossover of the τ_a versus voltage curves for the 0 and 5 aa linker mutants (Fig. 4 A).

Fig. 4 B shows the delays (*d*) as a function of voltage for the 10 (●), 5, and 0 aa linker mutant channels. Since *d* is the reciprocal value of the sum of all α_i ($i \neq j$), it is clear that one or more of the forward rate constants are affected by S3–S4 linker shortening. Surprisingly, the voltage dependence of *d* for the 0 aa linker mutant channel was found to be larger than that of the WT *Shaker*Δ and the rest of the linker mutant channels. It is possible for this channel that a transition with a large voltage dependence has become much slower than the rest of the forward rates.

Fig. 5 shows the voltage dependence of the deactivation kinetics obtained using the pulse protocol illustrated in the inset. In the range between −100 and −50 mV, the deactivation time constants are 6-, 3-, and 1.5-fold larger in the 0, 5, and 10 aa linker mutants than in the WT channel, respectively. The voltage dependence of the 0 aa linker mutant is essentially indistinguishable from the WT channel, and the equivalent number of gating charges related to channel deactivation, z_d, for the 5 aa linker mutant is 0.58 compared with 0.53 in the WT channel.

A Large Cole-Moore Shift Is Present in the 5 aa Linker Mutant

Cole and Moore (1960) found that K^+ currents were delayed by hyperpolarizing prepulses a phenomenon that has been dubbed the Cole-Moore shift. The initial lag of the ionic currents reflects the early transitions of the activation pathway. A large hyperpolarizing prepulse will populate those closed states further removed from the open state, which results in a longer lag in the activation of the ionic current. In *Shaker*Δ K^+ channels, an ~1-ms time shift of the ionic current onset is induced when the prepulse is varied from −150 to −50 mV (Stefani et al., 1994; Rodriguez et al., 1998). Fig. 6 A shows superimposed ionic current records for the 5 aa linker mutant elicited by a 50-mV test pulse for different conditioning prepulses ranging from −130 to −40 mV with the longest lag observed for the −130-mV conditioning pulse. The traces show unambiguously that the depolarizing prepulses produce a decrease in the time shift or delay of the onset of the ionic currents and that this delay is much more pronounced in the 5 aa linker mutant than in WT *Shaker* K^+ channels (see Stefani et al., 1994). In Fig. 6, B–D, we have plotted the time shift promoted by the prepulses indicated in the abscissa for the 10, 5, and

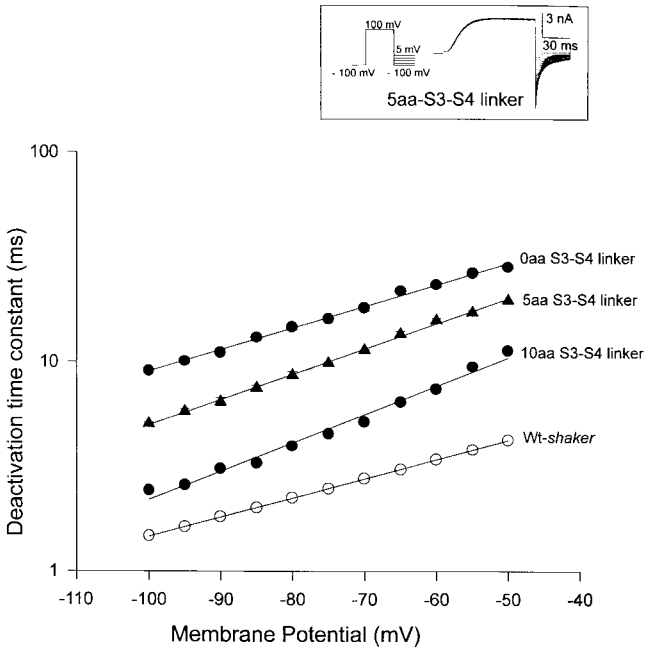

Figure 5. The time constants of current deactivation were obtained by fitting the tail currents after a 250-ms activating pulse to 15 mV as indicated in the pulse protocol shown in the inset. Time course was fitted with a single exponential. Solid lines are fit to the data using $\tau_d = C \exp(-ZV/RT)$, where τ_d is the deactivation time constant, C is a constant, and Z defines the voltage dependence of τ_d. The values of Z were: 0.53 ± 0.9, 0.8 ± 0.08, 0.58 ± 0.1, and 0.69 ± 0.08 for the WT, and 10, 5, and 0 aa linker mutants, respectively.

0 aa linker mutant channels. In 10 aa linker channels, we observed that an ~1-ms time shift of the ionic current onset was induced when the prepulse was varied from −150 to −40 mV. This value is very similar to the one obtained with the WT channel. In the case of the 5 aa linker channel, the shift obtained with a −40-mV prepulse was 12.4 ms, which is ~12-fold larger than the time shift found for WT *Shaker* K^+ channels (Rodriguez et al., 1998). Although smaller than the Cole-Moore shift found for the 5 aa linker mutant, the 0 aa linker mutant shows a pronounced delay in the ionic currents with hyperpolarization (Fig. 5 B). In this mutant, the shift obtained with a −40-mV prepulse was 8 ms.

Change in Gating Valence Induced by Complete S3–S4 Linker Removal

The next step was to determine whether the linker deletions modify the apparent number of gating charges per channel. If the S4 domain undergoes a large displacement during channel activation, this movement should be constrained by the linker length. Since the apparent number of charges per channel is the product of the valence z times the displacement δ that each charge undergoes, an abridgment of the S4 motion imposed by the shorter linker should be manifested as a decrease in $z\delta$.

To calculate the number of effective charges per channel, $z\delta$, we have applied the limiting slope method (Almers, 1978; Sigg and Bezanilla, 1997; see materials and methods). In this case, the voltage sensitivity of channel opening, measured at negative potentials in a range where the opening probability is low, yields a lower limit to $z\delta$. To increase the voltage resolution for the WT *Shaker*Δ K^+ and the linker mutant channels, we used slow ramp stimulation from −100 to 0 mV (Fig. 7; Noceti et al., 1996; Seoh et al., 1996). This method is adequate for obtaining a quasi steady state G-V relationship at potentials more negative than −50 mV. For larger depolarizations, conductance values are slightly underestimated due to the presence of a slow inactivation process. The steady state conditions were checked by varying the speed of the ramp and by testing the symmetry of the current in response to a symmetric triangular voltage wave. Fig. 7, A and E, confirmed the value of $z\delta$ obtained in previous studies for the WT *Shaker* K^+ channel (Zagotta et al., 1994b; Seoh et al., 1996; Noceti et al., 1996). A fit to the data at very negative potentials using Eq. 3 ($P_o \rightarrow 0$; Fig. 7 A) gave a $z\delta = 12.1$. To verify the validity of our assumption $P_o \rightarrow 0$, we determined the slope of the logarithm of the G-V curve at low open probabilities, and $z\delta$ at the different voltages was obtained using Eq. 4. When $z\delta$ is plotted as a function of V, it reaches a plateau that is equal to the actual value of the limiting slope (Fig. 7 E), giving a value very close to that obtained by the exponential fit (straight line). For the WT *Shaker* K^+ channels, we obtained a $z\delta = 12.5 \pm 0.62$ ($n = 5$), in reasonable agreement to the $z\delta = 12.3$ found by Schoppa et al. (1992) or the $z\delta = 12.8$ found by Noceti et al. (1997) and 12.6 found by Seoh et al. (1996). Essentially the same $z\delta$ was found for the 10 aa linker mutant, Fig. 7, B and F (12.7 ± 0.54).

We used the ramp method to determine the $z\delta$'s of the 5 aa (Fig. 7, C and G) and the 0 aa (D and H) linker mutants. Fig. 7 C is the conductance corresponding to the ionic current flowing through 5 aa linker mutant channels in response to a ramp from −90 to −20 mV (1.2 mV/s). The conductance values obtained for very negative voltages (−70 to −50) were fitted to Eq. 3 to approximate to the limit $P_o \rightarrow 0$. The calculated parameters of the fit were $A = 5 \times 10^{13}$ nS and $z\delta = 12.0$. We also calculated $z\delta$ at different voltages using Eq. 4 (Fig. 7 G) to obtain a $z(V)$ versus V curve. Fig. 7 C shows that $z\delta$ approaches a limiting value close to the fitted value obtained in Fig. 7 G (straight line). The average value for $z\delta$ in the 5 aa linker mutant was 12.3 ± 0.87.

Fig. 7, D and H, illustrates a limiting slope experiment in the 0 aa linker mutant channel with the same strategy as the experiments shown in Fig. 7, A–G. In this case, a slow ramp from −90 to −20 mV (1.2 mV/s) was used to induce the ionic current that was then converted into conductance (Fig. 7 D). Notice that for

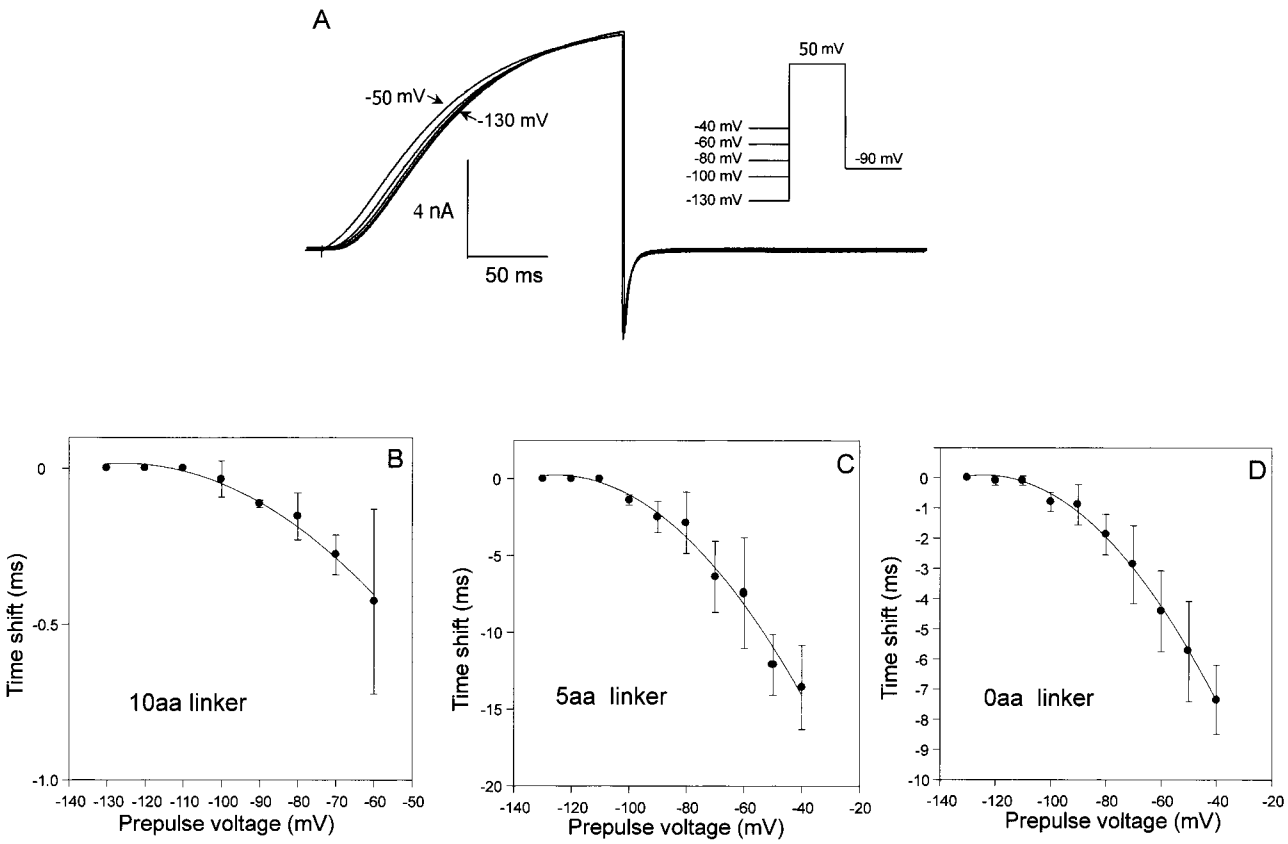

Figure 6. Kinetics of early transitions of the activation pathway using the Cole-Moore protocol. (A) Family of macroscopic ionic currents from 5 aa linker mutant channels elicited in response to the variable hyperpolarized prepulses shown in the pulse protocol followed by a 50-mV test pulse and a postpulse of −90 mV. The holding voltage was −90 mV. A P/−4 subtraction protocol was used. Data was filtered at 5 kHz and digitized every 100 μs. (B) Delay or time shift due to the hyperpolarized prepulses for the linker mutant channels calculated from current records was measured by displacing the current records along the time axis until the best superposition was obtained. Lines in these plots were drawn by eye.

both the 5 and 0 aa linker mutants, very slow ramps were used to attain a quasi steady state G-V curve, due to the slow activation kinetics showed by these two mutants (Fig. 2). The monoexponential fit to the initial part of the curve (−89 to −67 mV) produced the following parameters: $A = 4 \times 10^7$ nS and $z\delta = 5.21$. As for the wild type and 5 aa linker mutant channels, a clear plateau in the curve $z\delta$ versus voltage was observed, providing a good estimate of the total number of charges per channel displaced during activation. For the 0 aa linker mutant, the average $z\delta$ obtained from seven experiments was 5.6 ± 0.32.

Noise Analysis Reveals the Same P_o^{max} for WT Shaker and Mutant Channels

The maximum probability of opening for the WT *Shaker* K^+ channel was determined using nonstationary fluctuation analysis (Sigworth, 1980) and is in the range of 0.73–0.79 (Schoppa et al., 1992; Noceti et al., 1996; Seoh et al., 1996). To avoid complications arising from channel inactivation, we measured the number of channels (N) at different stimulating frequencies and used only those frequencies that did not modify N. Fig. 8, A–C, shows variance analysis in the 10 aa linker mutant channel. Fig. 8, A and B, shows the time course of the average current for a +120-mV pulse and the corresponding variance versus time plot. The noise fluctuations in Fig. 8 B have a biphasic time course that is a reflection of the channel open probability during the activation of the ionic current. The variance-mean current plot in Fig. 8 C was fitted to Eq. 2. The fitted parameters were, N = 10,080 channels and i = 0.95 pA (average i = 0.560.3, n = 5). The maximum open probability was obtained using the relation $P_o^{max} = I_{max}/iN$ and was 0.73. The average P_o^{max} calculated from five different cell-attached patches was 0.74 ± 0.03.

The maximum open probability for the 5 aa linker mutant was also estimated by nonstationary fluctuation analysis (Fig. 8, D–F). As with the 10 aa linker mutant, a parabolic relationship between the variance and the mean current was seen for the 5 aa linker mutant (Fig. 8 F), leading to accurate estimates of N and P_o^{max}. The solid line in Fig. 8 F is a fit to the variance–mean cur-

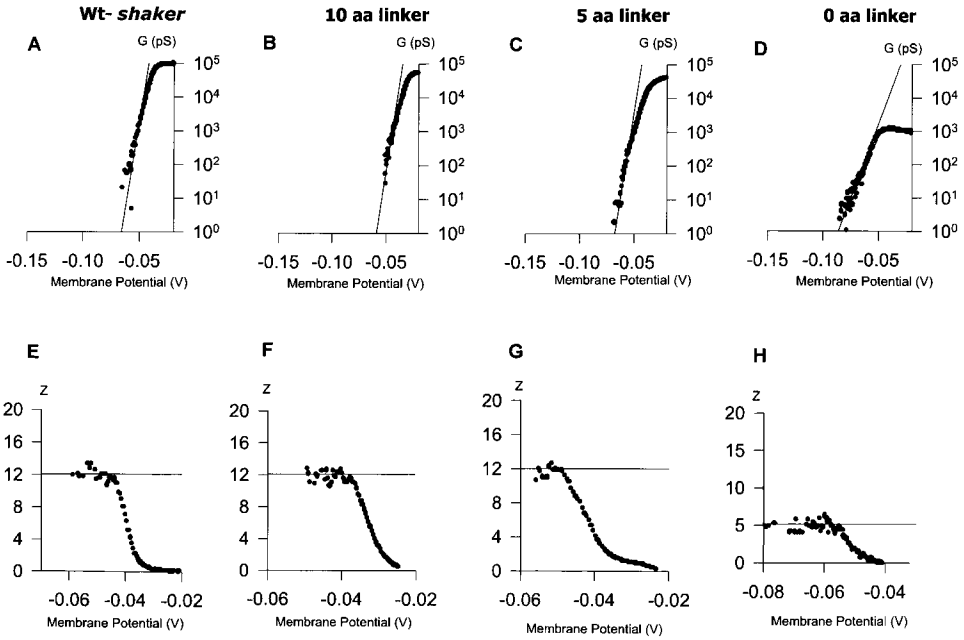

Figure 7. Limiting slope analysis in wild-type *Shaker*Δ and the S3–S4 linker mutant channels. (A–D) Semilogarithmic plot of the G vs. V relationship of the different mutants. The solid line indicates the fitting of the low probability data in order to determine the limiting value of *z*. (E–H) *z* vs. V plot of the corresponding mutants indicated above the A–D graphs. The solid line indicates the asymptotic value of *z* at very hyperpolarizing voltages obtained by the derivative with respect to the voltage of the monoexponential fit of the low probability data.

rent data with $N = 10{,}000$ channels, $i = 0.82$ pA (average $i = 0.730.2$, $n = 8$), and the calculated P_o^{max} was 0.75 (average $P_o^{max} = 0.76 \pm 0.05$). In the case of the 0 aa linker mutant channel, Fig. 8, G and H, shows the time course of the average current for a +120-mV pulse and the corresponding variance versus time plot. The solid line in Fig. 8 I is a fit to the variance–mean current data with $N = 890$ channels, $i = 0.36$ pA, (average $i = 0.540.3$, $n = 5$), and the calculated P_o^{max} was 0.73.

DISCUSSION

General

By inserting an epitope at different positions in the S3–S4 linker, Shih and Goldin (1997) determined that the minimum length of the linker was established to extend from amino acid 333 to 356. Shih and Goldin (1997) modeled the S3–S4 loop as the 30 amino acid region extending from amino acid ala328 to leu358,

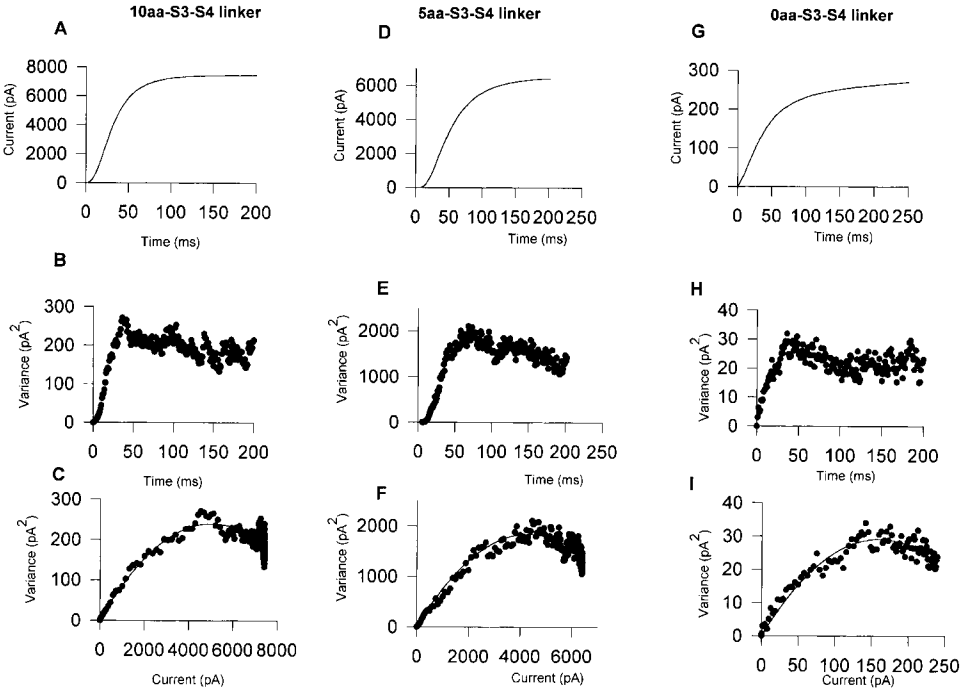

Figure 8. Variance analysis for three deletion mutants. (A,D, and G) Mean current traces obtained from 256 traces recorded with the patch technique from a holding potential of −100 mV to a test pulse potential of 120 mV. (B, E, and H) Time course of the variance. (C,F, and I) Variance versus current fitted to the function $\sigma^2 = iI(t) - I(t)^2/N$ (solid line). The mean maximum open probability (P_o^{max}) among the different mutants was 0.75.

and Wallner et al. (1996) defined the linker as the segment comprised of residues val330–ileu360. In the present study, we used the Wallner et al. (1996) definition to investigate the role of the S3–S4 loop.

The initial studies on the role of the S3–S4 linker performed by Mathur et al. (1997) showed only minor effects on the gating kinetics of the *Shaker*Δ by the introduction of point mutations in the *Shaker*Δ S3–S4 linker. Replacement of the *Shaker*Δ S3–S4 linker by the shorter (7 aa) linker of *Shaw* resulted in a three- to fourfold slowing down in the activation kinetics and in voltage shifts of the G-V curves of −13 mV. The linker definition of Mathur et al. (1997) extended from amino acid 333 and also included the serine located at position 357. Therefore, according to our linker definition, the linker still contained 13 amino acid residues even when they replaced the linker by the shorter, 7 aa linker of *Shaw*. We found that a mutant containing a linker as short as 10 aa (VVNRSMSLAI; Fig. 1) behaves as *Shaker*Δ in almost every respect except for slower speed of activation and deactivation (approximately twofold) and an increase in the slope (Table I), possibly due to an increase in positive cooperativity between subunits. Our results obtained using the 5 and 0 aa linker mutants are interesting in four respects. First, the main effect of the mutations was to slow down dramatically the activation kinetics and, to a much lesser extent, the speed of deactivation. Second, we expected to find an inverse relationship between speed of activation and linker length. Contrary to this expectation, we found that for voltages smaller than 60 mV the speed of activation was much slower in the 5 aa mutant linker than in the 0 aa mutant linker. However, for voltages >60 mV, the speed of activation of the 0 aa linker channel became slower than that of the 5 aa linker channel mutant. On the other hand, the speed of deactivation decreased inversely with S3–S4 linker length. Third, we found no evidence for a change in the gating valence for the 5 aa linker mutant, but in the 0 aa linker mutant the valence was halved. Fourth, the P_o^{max} was the same for *Shaker*Δ and the three mutants studied here.

The results obtained with the 5 aa S3–S4 linker mutant suggest that the linker length determines to a great extent the activation and deactivation channel kinetics. Moreover, the fact that in this mutant $z\delta$ and P_o^{max} are not altered suggests that a 5 aa linker is enough to allow for the full displacement of the voltage sensor and for normal coupling between voltage-dependent gating and pore opening.

Complete deletion of the S3–S4 linker in *Shaker*Δ K^+ channels greatly slows down the activation (∼45-fold) and deactivation (∼6-fold) kinetics compared with the wild-type *Shaker*Δ K^+ channel. These changes in channel gating kinetics are accompanied by a shift toward depolarizing voltages of the G-V curve. The shift to the right, measured at $P_o = 0.5$, induced by complete removal of the S3–S4 linker, is 45 mV. The change in free energy, ΔΔG, due to the linker deletion can be calculated using the expression:

$$K(0)_{0aa}/K(0)_{WT} = (-\Delta\Delta G/RT), \quad (8)$$

where the values of the equilibrium constants for the 0 aa linker [$K(0)_{0aa}$] and the WT *Shaker* [$K(0)_{WT}$] channel are those of Table I. K(0) values were obtained using Eq. 6 for the 0 aa linker and Eq. 7 for the wild type. Comparison of the K(0) values is meaningful since K(0) determines the equilibrium between resting or an active conformation of subunits in both cases. Different equations are needed since, for the WT *Shaker* K^+ channel, an extra process is required to reach the open state. Using Eq. 8, we obtain a $\Delta\Delta G = 1.2$ kcal/mol. This is a relatively small free energy change considering that the whole linker was deleted, and suggests that the conformational change of the S4 domain during activation does not involve extensive changes in sensor structure (see below). Most notably, deletion of the S3–S4 linker in *Shaker*Δ K^+ channels decreases the apparent gating valence from 13 e_o in *Shaker*Δ K^+ to 5.6 e_o, with no change in the P_o^{max}. The P_o^{max} is determined by transitions that have little or no voltage dependence; such transitions account for *Shaker's* single channel data at depolarized voltages and are outside of the activation path (Schoppa and Sigworth, 1998b). The fact that P_o^{max} is not affected by decreasing the S3–S4 linker length strongly suggests that these transitions are not modified in the S3–S4 linker mutants.

Possible Interpretations of the Decrease in zδ of the 0 aa Linker Mutant Channel

The studies of Cha and Bezanilla (1998) indicated the presence of an external water-filled vestibule lining the external region of the S4 segment. Fluorescence studies (Sørensen et al., 2000) suggest that the majority of the protein vestibule and the group(s) involved in quenching of fluorescence signals outside the S4 segment in the wild-type channel reside in the S3–S4 linker. Since deleting the S3–S4 linker promotes a reduction of ∼7 e_o, we conclude that despite the drastic reduction in total charge movement without modifying P_o^{max}, deletion of the S3–S4 linker did not affect the open position in the movement of the voltage sensor. Assuming that the S4 movement does not change in magnitude and a static S3 segment, an attractive hypothesis to explain this result would be that deletion of the linker makes the vestibule disappear (see Sørensen et al., 2000). If this is the case, we expect a decrease in the electrical distance (δ) traversed by some of the gating charges as pictured in Fig. 9 since after linker deletion they would be "inside" the dielectric region.

However, the decrease in zδ can also be due to the appearance of new open states connected by voltage-dependent rates induced by the linker deletion. The limiting slope method gives an estimate of the number of gating charges displaced between closed states and the first open state (Noceti et al., 1996; Sigg and Bezanilla, 1997). The charge moved between open states is not detected by the limiting slope method. We argue that this possibility is not very likely since, in the 0 aa linker mutant channel, about half of the charges are lost, implying that as much as 6 e_o are now being displaced between open states. For this to happen, we are forced to conclude that either a large amount of charge moves between a few open states, or that the linker deletion created a large number of open states where the "lost" gating charge is displaced. If the open states differ in their conductance, the variance versus mean ionic current data should deviate from the simple relation given in Eq. 1. The noise in the mean versus variance plot shown in Fig. 8 I makes it difficult to decide the presence of more than one conducting state.

It is also possible that the correct value of the total charge is not estimated properly because the applied voltages were not negative enough to reach a P_o low enough (Andersen and Koeppe, 1992; Schoppa et al., 1992; Bezanilla and Stefani, 1994; Zagotta et al., 1994a). As pointed out by Zagotta et al. (1994a), a test of having reached the true limiting slope is to plot zδ vs. P_o, where it is possible to visualize whether the estimate shows signs of reaching a limiting value. Fig. 7 H shows that zδ has reached a saturating value and that, with the caveat of the possible presence of several open states, this represents the total charge movement. In principle, it is possible to determine zδ by determining the total charge (Q) displaced and the number of channels (N) in the membrane area considered (Schoppa et al., 1992; Seoh et al., 1996; Noceti et al., 1996). However, until now we have failed to detect gating currents in the 0 aa linker mutant, most probably due to its very slow activation and deactivation kinetics. Since gating currents measurements are not yet possible for this mutant, we have used the Cole-Moore shift as a measure of the charge displacement at voltages more negative than −80 mV, which is the most negative voltage we used to estimate the charge with the limiting slope method. Although there is some Cole-Moore shift between −80 and −100 mV, the voltage dependence of the shift is so low that it is very unlikely that the missing six electron charges are mobilized at voltages more negative than −80 mV.

Kinetic Effects of Mutations

The analysis of the Cole-Moore shift of the ionic currents indicates that shortening the S3–S4 linker slows down transitions between closed states further removed from the open state. A quantitative comparison of the kinetics of the rate-limiting step of activation was obtained for *Shaker*Δ and the S3–S4 linker mutants. This was done by determining activation time constants from monoexponential fits of the rising phase of the test pulse currents. The analysis of the data shows that transitions in the activation pathway and near the open state are also greatly affected by shortening the linker to 5 or 0 amino acids. The 5 aa linker has an 88-fold slower activation than the *Shaker*Δ channel with no dif-

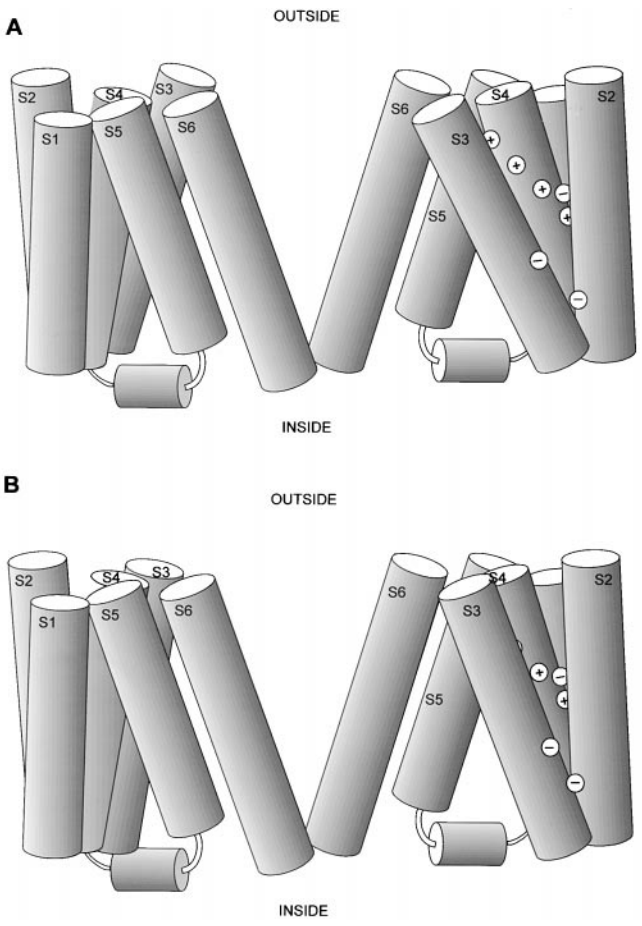

Figure 9. Model of the structure of all six segments of the *Shaker* K channel, which accounts for the observations described in the present study (Cha et al., 1999; Bezanilla, 2000). (A) Two subunits facing each other across the pore are shown. This allows the observation of the back face of the left subunit and the front face of the right subunit. Only the open configuration of the channel is shown. In this model, depolarization rotates the S4 segment in 180°, and charges that were facing the intracellular solution by being in the crevice formed by S1 and S5 are displaced towards the extracellular solution remaining in a water-filled crevice formed by segments S2 and S3. This requires an S4 movement of no more than a few Angstroms and explains why a 5 aa linker allows for the movement of all the channel gating charges. (B) When the whole S3–S4 linker is removed, the S3 and S4 segments are closer together, decreasing the width of the crevice formed by the S2 and S3 segments. This has the effect of widening the region where the electric field falls, with the consequent decrease in zδ.

ference in the voltage dependence (Fig. 4 A). In the case of the 0 aa linker mutant channel, the difference in activation speed with the *Shaker*Δ is 45-fold at 0 mV. The experimental protocols we used do not allow conclusions about the effect of the mutations on the backward rates in the activation pathway. However, Sørensen et al. (2000) found that both the on and off gating currents are very slow in the 5 aa linker mutant channel. This result suggests that decreasing the length of the linker restricts the movement of the gate in the direction of the deepest closed states.

If the ratio of activation time constants between the 5 aa linker and the *Shaker*Δ channel is assumed to be related to the difference in the energy necessary to displace the voltage sensor, ΔΔG, this energy amounts to 2.7 kcal/mol. In both the 5 and 0 aa linker channel mutants, the deactivation rate constant is much less affected than the activation process. Thus, a difference of sevenfold in deactivation rates between *Shaker*Δ and the 0 aa linker implies a $\Delta\Delta G = 1.2$ kcal/mol. The interpretation of this difference is obscured by the fact that the forward rate of the last transition, α_N, (Scheme III) is much faster than the rates of the previous forward rates, and even at −100 mV can have values comparable with the backward rate, β_N (Schoppa and Sigworth, 1998a).

In summary, shortening the S3–S4 linker to <10 amino acids appears to increase all the energy barriers separating the various kinetic transitions leading to channel opening. It is interesting to note that, with the exception of the extreme case of the 0 aa linker channel, these kinetic effects occurred in the absence of large changes in the voltage dependence of activation.

A Model Consistent with Results

The total charge per channel of the WT *Shaker*Δ estimated by three different methods is between 12.6 e_o (Seoh et al., 1996) and 13.6 (Aggarwal and MacKinnon, 1996); most of this charge is contained in the S4 domain. Moreover, the fact that the Q/N and the limiting slope method give the same $z\delta$ indicates that all the nonlinear charge in *Shaker*Δ K^+ channel is involved in channel opening (Seoh et al., 1996). Using neutralization mutants, Aggarwal and MacKinnon (1996) and Seoh et al. (1996) showed that arginines 362, 365, 368, and 371 contribute to the total gating charge. On the other hand, the results obtained with cysteine-scanning mutagenesis indicate that a conformational change of the S4 domain occurs during depolarization that results in a large change in the exposure of charged residues (Larsson et al., 1996; Yusaf et al., 1996; Baker et al., 1998). More recently, Starace and Bezanilla (1998, 1999) replaced the arginines by histidines (histidine-scanning mutagenesis) and found that these four charges change exposure from inside to outside upon depolarization. Thus, four of the seven positive charges contained in the S4 domain move from the inner to the outer surface of the membrane upon depolarization. Several models have been proposed to explain the conformational change that the S4 domain undergoes during the channel activation process. One model proposes a helical-screw motion of an α-helical S4 region (Durell and Guy, 1992; Catterall, 1996), which would imply an S4 segment displacement of 1.5 nm. This model also requires an S3–S4 linker long and flexible enough to allow for such a displacement. A second model involves a change in secondary structure from a helix in one state (for example, closed) to a loop in another state (helix-coil transition model; Guy and Conti, 1990; Sigworth, 1994; Aggarwal and MacKinnon, 1996). This model has a precedent in voltage-dependent gating of colicin channels. In this case, a large segment of the protein is transferred across the entire membrane upon activation (Slatin et al., 1994; Qiu et al., 1996).

Our results show that a very short linker is sufficient for the full displacement of the S4 segment. This result is inconsistent with the sliding helix model of Durell and Guy (1992), but can be interpreted in terms of a model in which charge displacement involves small movements of the voltage sensor (Papazian and Bezanilla, 1997) or in terms of the helix-coil transition model. As proposed, the helix-coil transition model also involves a large displacement of the charges contained in the S4 domain. Contrary to this expectation, recent evidence strongly suggests that the displacement of the gating charge is small and that the field is focused in a very thin low dielectric constant region. First, using lanthanide-based resonance energy transfer, Cha et al. (1999) determined that a residue in the S3–S4 linker moves ~3 Å between adjacent subunits. Second, histidine-scanning mutagenesis indicates that the transmembrane electric field is concentrated in a low dielectric region so narrow that the histidine 362 can bridge the hydrophobic span and gate open a H^+ channel (Starace and Bezanilla, 1999).

All the above evidence suggests that the S4 segment undergoes a rotation (Yellen, 1998; Cha et al., 1999; Bezanilla, 2000), as depicted in Fig. 9. In this model, the lining of the internal water-filled crevice is made up by the S1 and S5 transmembrane segments, and depolarization induces up to 180° rotation of the S4, exposing the charges to an external crevice formed by the S2 and S3 segments. Deleting the S3–S4 linker in this model would have the effect of narrowing the external crevice. Despite the fact that the charges would move the same absolute distance, some charge would not be able to cross the entire thickness of the low dielectric region. Therefore, as a consequence of this narrowing in the width of the external crevice, the number of apparent gating charges will decrease when the S3–S4 linker

is deleted, but the open probability would remain normal. In addition, the open state will be destabilized with respect to the wild-type channel because some of the charges would not become exposed to the solvent in the open position, producing a shift of the activation curve to the right.

We thank Dr. Albert Cha for critical reading of the manuscript and Luisa Soto for technical assistance.

This work was supported by Chilean grants FONDECYT 197-0739 (R. Latorre) and Cátedra Presidencial, a Human Frontier in Science Program grant (R. Latorre), and a group of Chilean companies (AFP Protection, CODELCO, Empresas CMPC, CGE, Gener S.A., Minera Escondida, Minera Collahuasi, NOVAGAS, Business Design Ass., and XEROX Chile) (R. Latorre), by National Institutes of Health grant GM30376 (F. Bezanilla), and a TWAS 1997 grant (C. Gonzalez).

Submitted: 2 July 1999
Revised: 5 January 2000
Accepted: 6 January 2000
Released online: 31 January 2000

REFERENCES

Aggarwal, S.K., and R. MacKinnon. 1996. Contribution of the S4 segment to gating charge in the *Shaker* K^+ channel. *Neuron*. 16: 1169–1177.

Almers, W. 1978. Gating currents and charge movements in excitable membranes. *Rev. Physiol. Biochem. Pharmacol*. 82:96–190.

Andersen, O., and R.E. Koeppe II. 1992. Molecular determinants of channel function. *Physiol. Rev*. 72:S89–S158.

Baker, O.S., H.P. Larsson, L.M. Mannuzzu, and E.Y. Isacoff. 1998. Three transmembrane conformation and sequence-dependent displacement of the S4 domain in *Shaker* K^+ channel gating. *Neuron*. 20:1283–1294.

Bezanilla, F. 2000. The voltage sensor in voltage-dependent ion channels. *Physiol. Rev*. 80:555–592.

Bezanilla, F., and E. Stefani. 1994. Voltage dependent gating of ionic channels. *Annu. Rev. Biophys. Biomol. Struct*. 23:819–846.

Catterall, W.A. 1996. Molecular properties of voltage-sensitive sodium channels. *Annu. Rev. Biochem*. 55:953–1021.

Cha, A., and F. Bezanilla. 1997. Characterizing voltage-dependent conformational changes in the *Shaker* K^+ channel with fluorescence. *Neuron*. 19:1127–1140.

Cha, A., and F. Bezanilla. 1998. Structural implications of fluorescence quenching in the *Shaker* K^+ channel. *J. Gen. Physiol*. 112:391–408.

Cha, A., G.E. Snyder, P.R. Selvin, and F. Bezanilla. 1999. Atomic scale movement of the voltage sensor in a potassium channel measured via spectroscopy. *Nature*. 402:809–813.

Cole, K.S., and J.W. Moore. 1960. Potassium ion current in the squid giant axon: dynamic characteristics. *Biophys. J*. 1:1–14.

Durell, S.R., and H.R. Guy. 1992. Atomic scale structure and functional models of voltage-gated potassium channels. *Biophys. J*. 62: 238–250.

Guy, H.R., and F. Conti. 1990. Pursuing the structure and function of voltage-gated channels. *Trends Neurosci*. 13:201-206.

Hodgkin, A.L., and A.F. Huxley. 1952. A quantitative description of membrane current and its application to conduction and excitation in nerve. *J. Physiol*. 117:500–544.

Koren, G., E.R. Liman, D.E. Logothetis, B. Nadal-Ginard, and H. Pess. 1990. Gating mechanism of a cloned potassium channel expressed in frog oocytes and mammalian cells. *Neuron*. 4:39–51.

Larsson, H.P., O.S. Baker, D.S. Dhillon, and E.Y. Isacoff. 1996. Transmembrane movement of the *Shaker* K^+ channel S4. *Neuron*. 16:387–397.

Ledwell, J.L., and R.W. Aldrich. 1999. Mutations in S4 region isolate the final voltage-dependent cooperative step in potassium channel activation. *J. Gen. Physiol*. 113:389–414.

Liman, E.R., J. Tytgat, and P. Hess. 1992. Subunit stoichiometry of mammalian K^+ channel determined by construction of multimeric cDNAs. *Neuron*. 9:861–871.

MacKinnon, R. 1991. Determination of the subunit stoichiometry of a voltage-activated potassium channel. *Nature*. 350:232–235.

Mannuzzu, L.M., M.M. Moronne, and E.Y. Isacoff. 1996. Direct physical measure of conformational rearrangement underlying potassium channel gating. *Science*. 271:213–216.

Mathur, R., J. Zheng, Y. Yan, and F. Sigworth. 1997. Role of the S3–S4 linker in *Shaker* potassium channel activation. *J. Gen. Physiol*. 109:101–199.

Noceti, F., P. Baldelli, X. Wei, N. Qin, L. Toro, L. Birnbaumer, and E. Stefani. 1996. Effective gating charges per channel in voltage-dependent K^+ and Ca^{2+} channels. *J. Gen. Physiol*. 108:143–155.

Papazian, D.M., and F. Bezanilla. 1997. How does a channel sense voltage? *News Physiol. Sci*. 12:203–210.

Qiu, X.-Q., K.S. Jakes, P.K. Kienker, A. Finkelstein, and S.J. Slatin. 1996. Major transmembrane movement associated with colicin Ia channel gating. *J. Gen. Physiol*. 107:313–328.

Rodriguez, B.M., D. Sigg, and F. Bezanilla. 1998. Voltage gating of *Shaker* K^+ channels. The effect of temperature on ionic and gating currents. *J. Gen. Physiol*. 112:223–242.

Schoppa, N.E., K. McCormack, M.A. Tanouye, and F.J. Sigworth. 1992. The size of gating charge in wild-type and mutant *Shaker* potassium channels. *Science*. 255:1712–1715.

Schoppa, N.E., and F.J. Sigworth. 1998a. Activation of *Shaker* potassium channels. I. Characterization of voltage-dependent transitions. *J. Gen. Physiol*. 111:271–294.

Schoppa, N.E., and F.J. Sigworth. 1998b. Activation of Shaker potassium channels. III. An activation model for wild-type and V2 mutant channels. *J. Gen. Physiol*. 111:313–342.

Seoh, S.-A., D. Sigg, D.M. Papazian, and F. Bezanilla. 1996. Voltage-sensing residues in the S2 and S4 segments of the *Shaker* K^+ channel. *Neuron*. 16:1159–1167.

Shih, T.M., and A.L. Goldin. 1997. Topology of the *Shaker* potassium channel probed with hydrophilic epitope insertions. *J. Cell Biol*. 136:1037–1045.

Sigg, D., and F. Bezanilla. 1997. Total charge movement per channel: the relation between gating displacement and the voltage sensitivity of activation. *J. Gen. Physiol*. 109:27–39.

Sigworth, F.J. 1980. The variance of sodium current fluctuations at the node of Ranvier. *J. Physiol*. 307:97–129.

Sigworth, F.J. 1994. Voltage gating of ion channel. *Q. Rev. Biophys*. 27:1–40.

Slatin, A., X.Q. Qiu, K.S. Jakes, and A. Finkelstein. 1994. Identification of a translocated protein segment in a voltage-dependent channel. *Nature*. 371:158–161.

Smith-Maxwell, C.J., J.L. Ledwell, and R.W. Aldrich. 1998. Role of the S4 in cooperativity of voltage-dependent potassium channel activation. *J. Gen. Physiol*. 111:399–420.

Sørensen, J.B., A. Cha, R. Latorre, E. Rosenman, and F. Bezanilla. 2000. Deletion in the linker between S3 and S4 in *Shaker* potassium channel reveals two quenching groups outside S4. *J. Gen. Physiol*. 115:209–221.

Starace, D., and F. Bezanilla. 1998. Accessibility studies of *Shaker* K channel S4 residues by histidine-scanning mutagenesis. *Biophys. J*. 74:A254. (Abstr.)

Starace, D., and F. Bezanilla. 1999. Histidine at position 362 causes inwardly rectifying H^+ conduction in *Shaker* K^+ channel. *Biophys. J*. 76:A266. (Abstr.)

Starace, D.M., E. Stefani, and F. Bezanilla. 1997. Voltage-dependent

proton transport by the voltage sensor of the *Shaker* K^+ channel. *Neuron*. 19:1319–1327.

Stefani, E., L. Toro, E. Perozo, and F. Bezanilla. 1994. Gating of *Shaker* K channels. I. Ionic and gating currents. *Biophys. J.* 66:996–1010.

Wallner, M., P. Meera, and L. Toro. 1996. Determinant for β-subunit regulation in high conductance voltage-activated and Ca^{2+}-sensitive K^+ channels: an additional transmembrane region at the N-terminus. *Proc. Natl. Acad. Sci. USA*. 93:14922–14927.

Yang, N., and R. Horn. 1995. Evidence for voltage-dependent S4 movement in sodium channels. *Neuron*. 15:213–218.

Yang, N., A.L. George, and R. Horn. 1996. Molecular basis of charge movement in voltage-gated sodium channels. *Neuron*. 16: 113–122.

Yellen, G. 1998. The moving parts of voltage-gated ion channels. *Q. Rev. Biophys.* 31:239–295.

Yusaf, S.P., D. Wray, and A. Sivaprasadarao. 1996. Measurement of the movement of the S4 segment during activation of a voltage-gated potassium channel. *Pflügers Arch.* 433:91–97.

Zagotta, W.N., and R.W. Aldrich. 1990. Voltage-dependent gating of *Shaker* A-type potassium channels in *Drosophila* muscle. *J. Gen. Physiol.* 95:29–60.

Zagotta, W.N., T. Hoshi, and R.W. Aldrich. 1994a. *Shaker* potassium channel gating. III: Evaluation of kinetic models for activation. *J. Gen. Physiol.* 103:321–362.

Zagotta, W.N., T. Hoshi, J. Dittman, and R.W. Aldrich. 1994b. *Shaker* potassium channel gating. II: Transitions in the activation pathway. *J. Gen. Physiol.* 103:279–319.